JOURNAL OF SOLID STATE CHEMISTRY **141,** 378–384 (1998)
ARTICLE NO. SC987956

Phase Diagram Investigations in the System Ba–Cu–O–Cl and Magnetic Properties of $Ba_3Cu_2O_4Cl_2$ and $Ba_2Cu_3O_4Cl_2$

K. Ruck, D. Eckert, G. Krabbes, M. Wolf, and K.-H. Müller

Institut für Festkörper und Werkstofforschung Dresden (IFW), Postfach, D-01171 Dresden, Germany

Received December 31, 1997; in revised form June 29, 1998; accepted July 7, 1998

The polythermal section at a constant composition of 20 mol% $BaCl_2$ of the quasi-ternary system $BaCl_2$–BaO–CuO_x was investigated at $p(O_2) = 0.21$ bar by means of DTA/TG and soaking experiments. Our results show the nature of incongruent decomposition reactions of the quaternary phases $Ba_3Cu_2O_4Cl_2$ and $Ba_2Cu_3O_4Cl_2$ at $T = 925°C$ (±5°) and $T = 975°C$ (±5°), respectively. Single crystals of both compounds were grown. Furthermore, field-dependent magnetic properties of $Ba_3Cu_2O_4Cl_2$ and $Ba_2Cu_3O_4Cl_2$ are measured at various temperatures. Both compounds contain two crystallographically different types of magnetic Cu atoms. $Ba_3Cu_2O_4Cl_2$ exhibits antiferromagnetic order with a Neél temperature T_N of about 20 K. A spin–flop transition is observed below T_N at a field of 2.6 T. $Ba_2Cu_3O_4Cl_2$ shows two antiferromagnetic transition temperatures at $T_{NI} \approx 337$ K and $T_{NII} \approx 33$ K. Below T_{NI} some spontaneous magnetization is observed. © 1998 Academic Press

INTRODUCTION

Six quaternary phases are known in the system Ba–Cu–O–Cl (Fig. 1). With regard to the Cu–O sublattice these compounds show different structural features. The high-pressure phase $Ba_2CuO_2Cl_2$ (1) is a build up of planar CuO_2 planes, which are known from the high-T_c superconductors. The structurally related compound $Ba_2Cu_3O_4Cl_2$ (2, 3) contains an additional Cu atom leading to planar Cu_3O_4 planes. $Ba_3Cu_2O_4Cl_2$ (4) exhibits one-dimensional folded chains and $Ba_9Cu_7O_{15}Cl_2$ (5) contains isolated ring-shaped units. The structural variety of this substance class leads to a wide array of interesting physical properties, which have become more and more the focus of interest in the past few years (e.g., 6–11).

Nevertheless, information about the phase equilibria of these compounds, which are important for preparation and crystal growth, is poor. Therefore, phase diagram investigations including the nature of decomposition reactions of the quaternary phases $Ba_2Cu_3O_4Cl_2$ and $Ba_3Cu_2O_4Cl_2$ are discussed in the present work.

Furthermore, we report on the magnetic properties of both compounds. Whereas $Ba_2Cu_3O_4Cl_2$ and the related Sr compound are well investigated (but not understood in detail (8–10)), the properties of $Ba_3Cu_2O_4Cl_2$ have so far been unknown.

EXPERIMENTAL

The samples were synthesized by conventional solid state techniques using BaO_2 (p.a., Merck), CuO (99.99%, MaTeck), and $BaCl_2$ (ultrapure, Alpha). After being mixed in stoichiometric amounts the powders were prereacted under Ar atmosphere for 8 h at 500°C (samples with CuO content <40 mol%) or at 700°C (samples with CuO content ≥ 40 mol%). Also, depending on the composition the final sintering step was carried out under an oxygen partial pressure of 0.21 bar at temperatures between 500 and 930°C. Hydrolysis and the formation of carbonates is favored during these processes, especially in the BaO-rich region of the phase diagram. To minimize these influences a mixed gas of 79 vol% N_2 and 21 vol% O_2 was used.

$Ba_2Cu_3O_4Cl_2$ is prepared monophasic by sintering the prereacted powder at 930°C for 48 h. Nearly single-phase $Ba_3Cu_2O_4Cl_2$ was obtained after annealing the prereacted compound at 700°C for 10 h. This product always contains traces of $BaCuO_2$ and $BaCO_3$ detected by X-ray analysis. All the other samples with nominal compositions on the discussed polythermal section are prepared impurity free.

Thin-layered $Ba_3Cu_2O_4Cl_2$ is green-colored. The compound is hygroscopic, but can be kept in dry air for several months. Direct contact with water leads to a quick hydrolysis forming a light-blue product. Similar observations have been described by Hien *et al.* (12) considering $Sr_2CuO_2Cl_2$. The black-colored $Ba_2Cu_3O_4Cl_2$ is less sensitive against moisture compared to $Ba_3Cu_2O_4Cl_2$, an analogous hydrolysis is not observed.

Single crystals of $Ba_2Cu_3O_4Cl_2$ were grown from the prereacted pure compound. This method becomes possible because of the direct neighborhood of the compound to its primary crystallization field in the phase diagram (Fig. 2). The powder was heated to 1040°C in alumina crucibles. This temperature was held for 1 h to homogenize the melt

0022-4596/98 $25.00

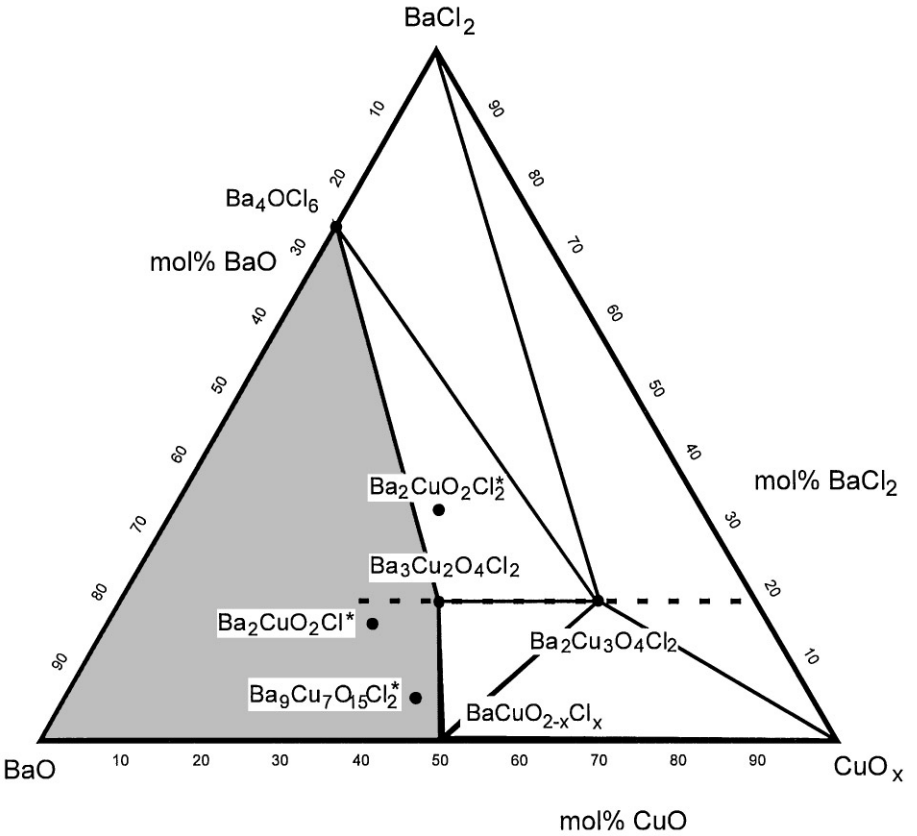

FIG. 1. Representation of the known quaternary phases into the quasi-ternary system $BaCl_2$–BaO–CuO_x. The phase compatibilities of the subsolidus region at $T \approx 800°C$ and $p(O_2) = 0.21$ bar are drawn. Compounds marked by * are not stable at these conditions. The gray area represents the field, where a partial melt is already formed at present conditions. The dashed line marks the polythermal section investigated in this work.

and was then slowly reduced to 800°C. To minimize the influence of evaporation of copper(I)chlorides an optimized relation between surface and amount of the melt was necessary. Besides single crystals of $Ba_2Cu_3O_4Cl_2$, the resulting product also contains small amounts of CuO, which can be detected by X-ray analysis.

In the case of $Ba_3Cu_2O_4Cl_2$, single crystals were obtained by a flux-method using $BaCl_2$ in a molar ratio of 5 : 1. After homogenization at 970°C the melt was slowly cooled to 700°C. $Ba_2Cu_3O_4Cl_2$ crystallizes first on the bottom of the crucible, single crystals of $Ba_3Cu_2O_4Cl_2$ are formed on the surface.

The crystals of both compounds are plate-like. Their average size after the mechanic isolation amounts to about 1–3 $mm^2 \times 0.1$ mm.

Phase diagram investigations are performed both in the subsolidus region and near the liquidus surface. In order to separate the solid phases from the coexisting melt, soaking experiments (13) were used. In detail, the samples were annealed at different temperatures for 15–24 h using $BaZrO_3$ as an inert material, which absorbs the liquid. The residual solid phases were characterized by EDX-measurements (EDAX System) and X-ray diffraction.

The powder patterns were obtained on a diffractometer PW 1820 (Philips) with monochromated Co$K\alpha$-radiation ($\lambda = 1.7903$ Å) in a 2θ range between 15° and 120° with a step width of 0.05°. Silicon was used as an internal standard. Single crystals were characterized and oriented by X-ray precession method.

The weight change of the samples was studied with a thermobalance TGA7 (Perkin–Elmer), DTA measurements were performed with a DTA/TG 92 (Setaram) at $p(O_2) =$ 0.21 bar.

The magnetic measurements on single crystals were carried out in a SQUID-magnetometer with a field up to 5 T in a temperature range between 1.7 and 400 K.

RESULTS AND DISCUSSION

1. Phase Diagram Investigations

Related to the quasi-ternary phase diagram (schematically represented by Fig. 1) the investigated polythermal section runs along a constant composition of 20 mol%

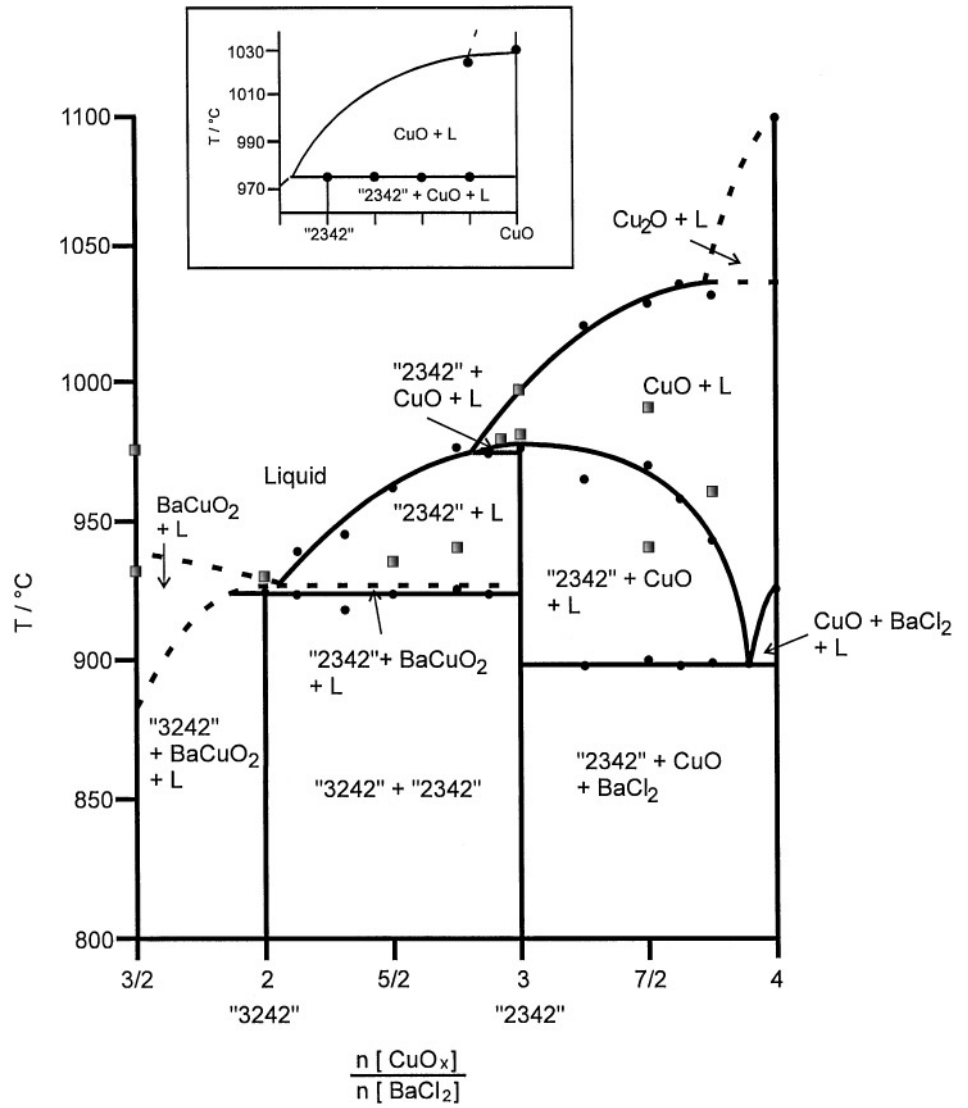

FIG. 2. Polythermal section along the nominal compositions $Ba_{3.5}Cu_{1.5}O_4Cl_2$–"3242"–"2342"–$Ba_{1.0}Cu_{4.0}O_4Cl_2$ at $p(O_2) = 0.21$ bar. The numbers written in quotation marks correspond to the formulas $Ba_3Cu_2O_4Cl_2$ or $Ba_2Cu_3O_4Cl_2$. The small picture shows the peritectic decomposition of $Ba_2Cu_3O_4Cl_2$ on the polythermal section $Ba_2Cu_3O_4Cl_2$–CuO.

$BaCl_2$. This section is shown in Fig. 2. The solid circles represent the temperatures of phase transitions determined by DTA measurements, the squares correspond to phase analysis via soaking experiments represented in Table 1.

The most important result of these investigations is the determination of the natures of decomposition reactions under equilibrium conditions for the two quaternary phases $Ba_3Cu_2O_4Cl_2$ and $Ba_2Cu_3O_4Cl_2$.

$Ba_3Cu_2O_4Cl_2$ is stable in 0.21 bar O_2 up to 925°C ($\pm 5°$). At this point the compound decomposes peritectically following

$$Ba_3Cu_2O_4Cl_2 \rightleftarrows \alpha BaCuO_2 + \beta Ba_2Cu_3O_4Cl_2 + \chi L + \delta O_2. \quad [1]$$

According to the phase rule,[1] the number F of free thermodynamic variables becomes one indicating a univariant reaction. Because the eutectic temperature of the quasi-binary system $BaCuO_2 + Ba_2Cu_3O_4Cl_2$ is close to the decomposition temperature of $Ba_3Cu_2O_4Cl_2$, the stability field of these residual phases [1] becomes narrow and therefore undetectable by DTA measurements. Nevertheless, supplementary phase investigations on the compatibility line $Ba_3Cu_2O_4Cl_2$–Ba_4OCl_6 revealed the formation of $Ba_2Cu_3O_4Cl_2$, $BaCuO_2$, and liquid as decomposition products. This result gives evidence for the proposed

[1] $F + P = C + 2$; F is the number of free thermodynamic variables, P is the number of phases, and C is the number of components.

TABLE 1
Residual Solid Phases in the Polythermal Section (Fig. 2) Determined by Soaking Experiments

n [CuO_x]/n[$BaCl_2$]	T [°C]	Residual solid	Method
15/4	960	CuO	X-ray
7/2	940	"2342,"[a] CuO	X-ray
7/2	985	CuO	X-ray
3 ("2342")[a]	980	CuO	EDX
3 ("2342")[a]	995	Liquid	
29/10	975	CuO	EDX
11/4	940	"2342"[a]	EDX
5/2	935	"2342"[a]	X-ray
2 ("3242")[a]	930	$BaCuO_2$	EDX
3/2	930	$BaCuO_2$	X-ray
3/2	975	Liquid	
3/2[b]	700	"3242"[a] $BaCuO_2$	X-ray
1[b]	700	$BaCuO_2$	X-ray

[a] The numbers written in quotation marks correspond to the formulas $Ba_3Cu_2O_4Cl_2$ or $Ba_2Cu_3O_4Cl_2$, respectively.
[b] These experiments are not shown in Fig. 2.

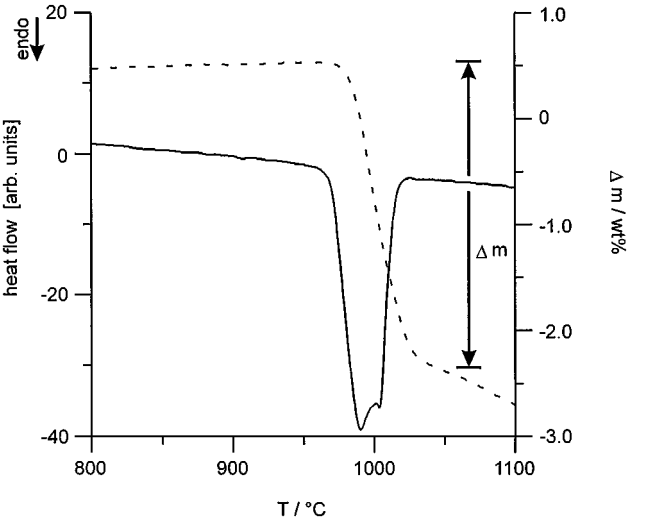

FIG. 4. DTA (solid line)/TG measurement (dashed line) of $Ba_2Cu_3O_4Cl_2$ at $p(O_2) = 0.21$ bar.

polythermal section. A univariant reaction between $Ba_3Cu_2O_4Cl_2$ and Ba_4OCl_6 that led to the disappearence of this compatibility line and the formation of $Ba_2Cu_3O_4Cl_2$ and liquid seems to be a possible explanation.

The complete melt is formed in a rather narrow temperature range. It is always accompanied by a weight loss of 1.3 wt% as detected by thermogravimetric analysis, which corresponds to 0.5 O per formula unit (Fig. 3).

$Ba_2Cu_3O_4Cl_2$ is found to be stable in 0.21 bar O_2 up to 975°C (±5°). At this temperature it also shows a peritectic decomposition behavior

$$Ba_2Cu_3O_4Cl_2 \rightleftarrows \alpha CuO + \beta L + \chi O_2. \qquad [2]$$

The peritectic reaction was also verified by DTA-investigations of the quasi-binary system CuO–$Ba_2Cu_3O_4Cl_2$. A weight loss of 2.9 wt%, which occurs during the melting process of $Ba_2Cu_3O_4Cl_2$ corresponds to 1.0 O per formula unit (Fig. 4).

According to Fig. 2, the liquidus temperature of $Ba_2Cu_3O_4Cl_2$ is lowered as the CuO content rises. This is due to a univariant reaction between the phases $Ba_2Cu_3O_4Cl_2$, and $BaCl_2$ which occurs under an oxygen partial pressure of 0.21 bar at a temperature of 900°C

$$\alpha Ba_2Cu_3O_4Cl_2 + \beta BaCl_2 \rightleftarrows \chi CuO + \delta L + \varepsilon O_2. \qquad [3]$$

The weight loss by further heating of the homogeneous melt of both compounds (Figs. 3 and 4) is caused by the evaporation of volatile CuCl, the vapor pressure of which is raised in the BaO-rich region. However, the above-mentioned TG-results, showing only a loss of oxygen until a complete melt has been formed, verify the proposed polythermal section also at higher temperatures. On the other hand, the loss of CuCl indicates that phase equilibria above the liquidus surface become dependent on the partial pressure of $(CuCl)_n$, as it is typical for CuCl as constituent of the melt (14).

Nevertheless, after longer sintering processes, impurity phases are found especially at the surface of the samples, which correspond to the expected decomposition products. Therefore, an optimized preparation path with regard to reaction time and temperature must always be found.

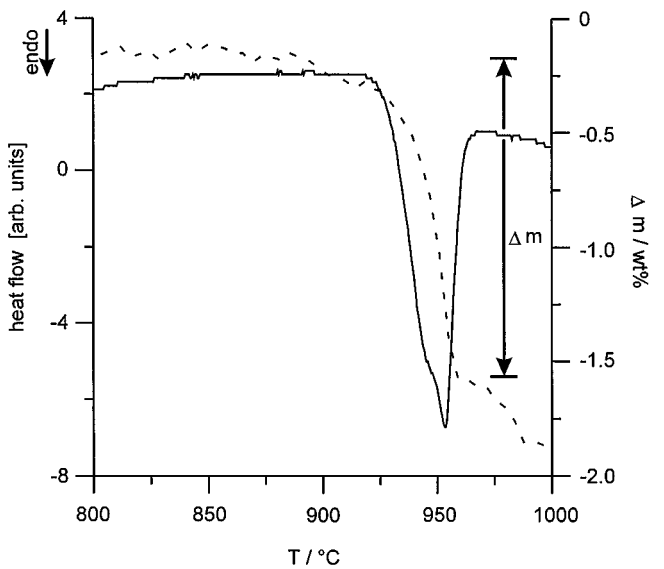

FIG. 3. DTA (solid line)/TG measurement (dashed line) of $Ba_3Cu_2O_4Cl_2$ at $p(O_2) = 0.21$ bar.

2. Magnetic Properties

$Ba_3Cu_2O_4Cl_2$ contains one-dimensional folded Cu_2O_4-chains along [100] with alternating cis- and trans- links between the square planar CuO_4 units yielding in Cu–O–Cu bond angles below 90° (4) (Fig. 5). The Cu–Cu distance along the chain direction is 2.435(1) Å (15), which is very short compared to the other known copper oxides (e.g., $Bi_2CuO_2 = 2.92$ Å (16) or $Li_2CuO_2 = 2.84$ Å (17)). Nevertheless, direct cation–cation interaction is not possible because of the filled dz^2 and dxy orbitals of square planar and pyramidal coordinated Cu^{2+}. Hence, the compound would be a candidate for ferromagnetic interactions applying the superexchange rules (18).

The expected localized state of Cu^{2+} is confirmed by the isolating behavior of the compound as well as by the results obtained from high-resolution X-ray photoemission study (11).

Figure 6 represents the field dependence of the specific magnetization of $Ba_3Cu_2O_4Cl_2$ measured on a single crystal, for various temperatures, along the a axis. For $T > 20$ K the magnetization is proportional to the applied field up to 5 T and shows a strong temperature dependence as expected for a paramagnetic behavior. In this temperature range the values can be well fitted by the Curie–Weiss law $\chi = C/(T - \theta)$, yielding a paramagnetic moment of 2.0 μ_B per Cu atom, which is higher than the value corresponding to $S = 1/2$ for Cu^{2+}. The paramagnetic Curie temperature θ of about 21 K indicates the presence of ferromagnetic interaction between the Cu spins. However, the dominating ordering is antiferromagnetic with a Néel temperature below 20 K. At high fields the ordering is strongly isotropic. Parallel to the a axis a sharp drop of the magnetization is observed at the critical field $\mu_0 H_{crit} \approx 2.6$ T. Below H_{crit}, the antiferromagnetic-ordered moments arrange parallel to the a axis, which is derived from the low values of magnetization and the large influence of temperature compared to the applied field. Above H_{crit}, the behavior is vice versa, indicating a spin configuration perpendicular to the applied field. Due to these results the metamagnetic transition is identified as a spin–flop transition. It occurs only parallel to the a axis, along the b or c axes the field-vs-magnetization curves (not shown here) are straight lines over the whole measured range of the magnetic field.

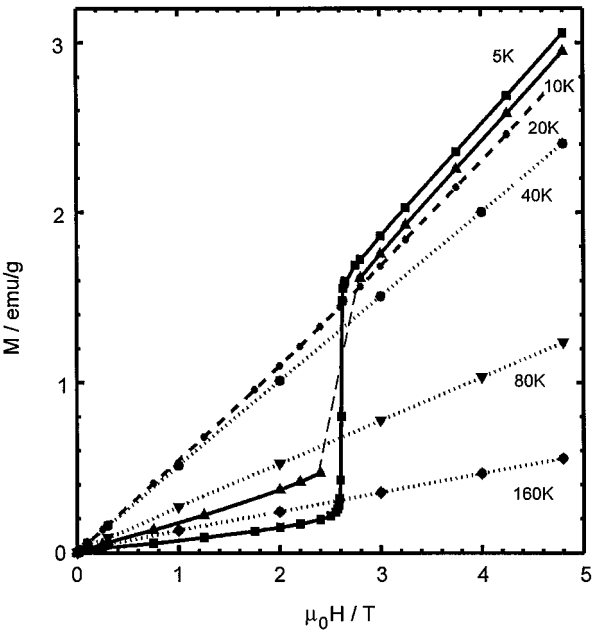

FIG. 6. Field dependence of the specific magnetization M of a $Ba_3Cu_2O_4Cl_2$ single crystal, measured for various temperatures with the field parallel to the a axis.

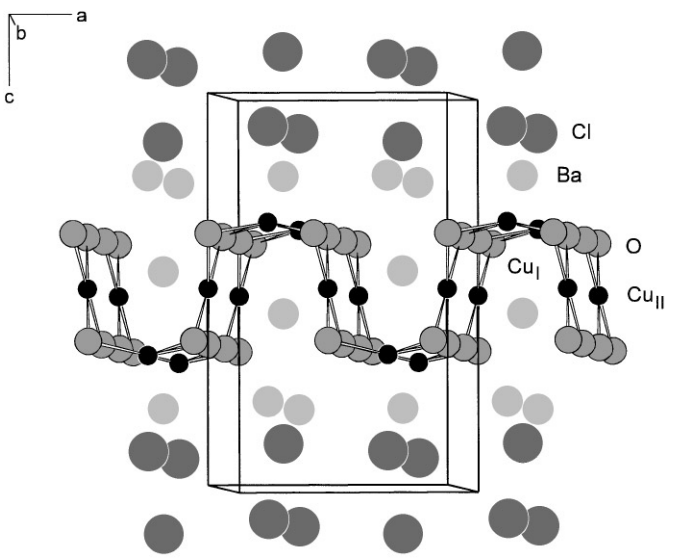

FIG. 5. Crystal structure of $Ba_3Cu_2O_4Cl_2$ (space group *Pmma*; $a = 6.648(1)$, $b = 5.991(1)$, $c = 10.585(1)$ Å). The folded Cu_2O_4 chains contain two crystallographically different types of copper atoms.

Obviously, for explanation of the magnetic behavior of $Ba_3Cu_2O_4Cl_2$ a three-dimensional coupling of the chains must be taken into consideration.

The crystal structure of $Ba_2Cu_3O_4Cl_2$ contains planar Cu_3O_4 planes (Fig. 7) with two crystallographically different kinds of copper atoms. Both are square-planar coordinated with four oxygen atoms. Cu_I-type atoms form a network with oxygen atoms via a Cu_I–O–Cu_I bond angle of 180°. They constitute 2/3 of the whole Cu content in the unit cell. The Cu_{II}-type atoms are connected only with Cu_I bridged by oxygen atoms. They form a Cu_{II}–O–Cu_I angle of 90° (2, 3). This arrangement results in the occurrence of two different magnetic subsystems. As can be expected from the superexchange rules of the Cu_I–O–Cu_I interactions, the compound is reported to be a $S = 1/2$ square lattice Heisenberg antiferromagnet (10).

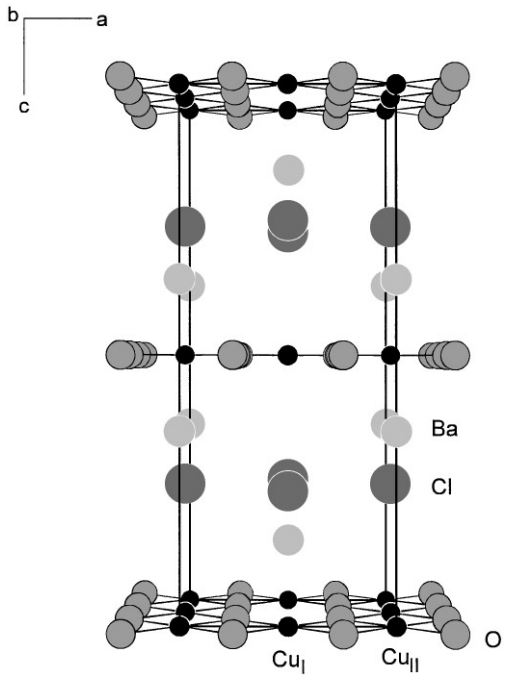

FIG. 7. Crystal structure of $Ba_2Cu_3O_4Cl_2$ (space group $I4/mmm$; $a = 5.5156(1)$, $c = 13.8221(3)$ Å). The Cu_3O_4 planes contain two crystallographically different types of copper atoms.

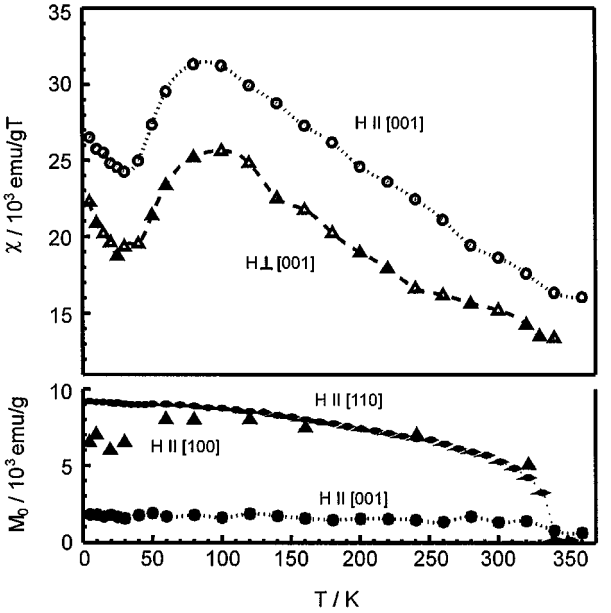

FIG. 8. Temperature dependence of the susceptibility ψ and spontaneous magnetization M_0 of a $Ba_2Cu_3O_4Cl_2$ single crystal.

The magnetization of an oriented single crystal of $Ba_2Cu_3O_4Cl_2$ was measured field dependent at various temperatures. The slope yields the suszeptibility χ, which is drawn in Fig. 8. Within the temperature range where both oxychlorides order antiferromagnetically, the specific magnetization of $Ba_2Cu_3O_4Cl_2$ was found to be more than one order of magnitude smaller compared to the values measured for $Ba_3Cu_2O_4Cl_2$ perpendicular to the a axis or at fields above $H_t = 2.6$ T.

The antiferromagnetic ordering of Cu_I-type atoms occurs below 337 K. This is connected with the appearance of weak ferromagnetism M_0 (Fig. 8), which is observed for H$\|$ plane in accordance with the result by Ito *et al.* (10). At 33 K the Cu_{II}-type atoms order antiferromagnetically corresponding to a minimum in the χ versus T curve. Contrary to the literature data, a significant decrease of the spontaneous magnetization for H$\|$ [100] compared to M_0 for H$\|$ [110] can be observed.

The origin of the weak ferromagnetism is discussed (controversially) either as a Dzyaloshinsky–Moriya type (10) or as an anisotropic pseudodipolar interaction between antiferromagnetic Cu_I and paramagnetic Cu_{II} atoms (8). However, these two theories are able to explain only the magnetic behavior between T_{NI} and T_{NII}. The reason for the further existence of M_0 below T_{NII} is not yet clear (Fig. 8). The magnetic properties of both compounds will be discussed in more detail in (19).

ACKNOWLEDGMENTS

Mrs. W. Höppner is gratefully thanked for her help in the preparation of the samples and Mrs. Ch. Heße for performing the XRD analysis. Financial assistance from the Fonds der Chemischen Industrie is gratefully acknowledged.

REFERENCES

1. T. Tatsuki, A. Tokiwa-Yamamoto, T. Tamura, Y. Moriwaki, X.-J. Wu, S. Adachi, and K. Tanabe, *Physica C* **265,** 323 (1996).
2. R. Kipka and Hk. Müller-Buschbaum, *Z. Anorg. Allg. Chem.* **419,** 58 (1976).
3. W. Pitschke, G. Krabbes, and N. Mattern, *Powder Diffraction* **10**(4), 282 (1995).
4. R. Kipka and Hk. Müller-Buschbaum, *Z. Anorg. Allg. Chem.* **422,** 231 (1976).
5. R. Kipka and Hk. Müller-Buschbaum, *Z. Naturforsch. B* **31,** 1067 (1976).
6. H. C. Schmelz, M. Knupfer, M. S. Golden, O. Knauff, T. Boeske, S. Haffner, G. Krabbes, A. Müller, G. Reichardt, and J. Fink, *Physica B* **230–232,** 850 (1997).
7. L. L. Miller, X. L. Wang, S. X. Wang, C. Stassis, D. C. Johnston, J. Faber, and C.-K. Loong, *Phys. Rev. B* **41**(4), 1921 (1990).
8. F. C. Chou, Amnon Aharony, R. J. Birgeneau, O. Entin-Wohlman, M. Greven, A. B. Harris, M. A. Kastner, Y. J. Kim, D. S. Kleinberg, Y. S. Lee, and Q. Zhu, *Phys. Rev. Lett.* **78,** 535 (1997).
9. K. Yamada, N. Susuki, and J. Akimitsu, *Physica B* **213–214,** 191 (1995).
10. T. Ito, H. Yamaguchi, and K. Oka, *Phys. Rev. B* **55,** R684 (1997).
11. T. Böske, K. Maiti, O. Knauff, K. Ruck, M. S. Golden, G. Krabbes, J. Fink, T. Osafune, N. Motoyama, H. Eisaki, and S. Uchida, *Phys. Rev. B* **57**(2), 1 (1998).
12. N. T. Hien, J. J. M. Franse, J. J. M. Pothuizen, T. W. Li, and A. A. Menovsky, *J. Cryst. Growth* **171,** 102 (1997), and references therein.

13. N. Nevriva, P. Holba, S. Durcok, D. Zemanova, E. Pollert, and A. Triska, *Physica C* **157,** 334 (1989).
14. G. Krabbes and H. Oppermann, *Z. Anorg. Allg. Chem.* **435,** 33 (1977).
15. K. Ruck, G. Krabbes, and M. Ruck, *in* "Proceedings of 5th Nato Advanced Research Workshop: High-Temperature Superconductors and Novel Inorganic Materials Engineering, Moscow," Kluwer Academic, in press.
16. R. Arpe and Hk. Müller-Buschbaum, *Z. Anorg. Allg. Chem.* **426,** 1 (1976).
17. R. Hoppe and H. Rieck, *Z. Anorg. Allg. Chem.* **379,** 157 (1970).
18. J. B. Goodenough, *Prog. Solid State Chem.* **5,** 145 (1972).
19. D. Eckert, K. Ruck, M. Wolf, G. Krabbes, and K.-H. Müller, *J. Appl. Phys.* **83,** 7240 (1998).